ISSN Number: 2454-2024(Online)
International Journal of Technical Research & Science

AI-DRIVEN MPPT TECHNIQUES FOR ENHANCING OFF-GRID SOLAR PV SYSTEM EFFICIENCY

Pandya Vatsalkumar[1], Kapil Parikh[2]
E-Mail Id: vapandya27@gmail.com
Department of Electrical Engineering, SITE, Nathdwara, Rajasthan, India

Abstract- This paper explores the increasing role of photovoltaic (PV) systems in power networks due to their economic and technical benefits. PV systems, used in sectors like electric vehicles and residential applications, are expected to supply up to 45% of global energy demand. However, their output is influenced by factors like irradiance and temperature, emphasizing the need for efficient maximum power point tracking (MPPT). This study presents an Adaptive Neuro-Fuzzy Inference System (ANFIS)-based MPPT controller for a DC-DC converter with a 2.5 kW PV array. The ANFIS controller combines neural networks and fuzzy logic, providing enhanced performance with minimal complexity. Simulations show that ANFIS outperforms traditional AI-based MPPT methods, achieving superior results in dynamic conditions and showing zero mean squared error. This approach highlights the potential of ANFIS for optimizing PV system performance in renewable energy applications.

Keywords: ANFIS, ANN, BR, SCG, MPPT, DC to DC boost converter

1. INTRODUCTION

Renewable energy sources (RES) are increasingly relied upon as sustainable alternatives to conventional energy systems, addressing concerns over fossil fuel depletion, global warming, greenhouse gas emissions, and environmental pollution. Among RES, photovoltaic (PV) energy is gaining significant traction due to its potential for clean energy generation. Photovoltaic systems, however, face challenges related to fluctuating environmental conditions such as solar irradiance and temperature, which affect their efficiency. Artificial Intelligence (AI)-based models offer a solution to these challenges, particularly in Maximum Power Point Tracking (MPPT) for PV systems. The AI-based MPPT models, especially those utilizing Artificial Neural Networks (ANN), allow for fast and accurate MPP tracking without requiring complex mathematical relations between system parameters like output power, irradiance, and temperature. ANN-based algorithms offer several advantages, such as the ability to approximate continuous nonlinear functions using multilayer networks with hidden layers. These networks are parallel in design and simple in structure, improving processing efficiency. Furthermore, ANNs generalize learning and offer predictive capabilities, thus reducing the time required for online learning and improving overall efficiency in tracking the MPP.

This paper focuses on comparing two AI-based techniques for MPPT: the ANN and Adaptive Neuro-Fuzzy Inference System (ANFIS). Both techniques are designed to track the MPP under nonlinear, variable solar irradiation. The study finds that ANFIS outperforms ANN in terms of settling time, efficiency, accuracy, and response speed, making it a more effective solution for PV systems. As solar PV energy becomes a more integral part of global energy networks, effective forecasting and performance optimization are critical. Accurate MPPT algorithms help minimize performance fluctuations due to environmental changes, thus improving reliability and reducing maintenance costs in PV systems. This paper also analyzes the performance of MPPT techniques such as Perturb and Observe (P&O), Incremental Conductance (INC), and Fuzzy Logic Control (FLC), highlighting their strengths and limitations in PV power generation.

2. MATHEMATICAL MODELING OF SOLAR PHOTOVOLTAIC ARRAY

This modeling approach aims to help users better understand the I–V and P–V characteristic curves of PV modules. It can also be used to predict the behavior of solar PV cells, modules, and arrays under varying environmental conditions and physical parameters. A solar cell is represented by a current source I_{ph}, which is the photocurrent of the cell, along with the shunt resistance R_{sh} and series resistance R_s, which are the inherent resistances of the cell. The shunt resistance R_{sh}, represents leakage current, while the series resistance R_s accounts for internal resistance to current flow. Typically, R_{sh} is very high, and R_s is very low, so these resistances are often neglected to simplify the analysis. In practice, PV cells are connected in series or parallel to form PV arrays, which generate electricity in PV power systems. Fig. 2.1 illustrates the equivalent circuit of a PV cell, while Fig. 2.2 shows the equivalent circuit for a PV array. The Simulink model of the Solar PV system is depicted in Fig. 2.3.

The current-voltage characteristic equation of a solar cell is given by:

Module photo-current Iph is expressed as:

$$I_{ph} = \left[I_{sc} + K_i \left(T - 298 \right) \right] * I_r / 1000 \qquad \ldots 1.$$

@2017, IJTRS All Right Reserved

Here,

I_{ph} : Photocurrent (A), I_{sc} : Short circuit current (A), K_i : Short-circuit current of cell at 25 °C and 1000 W/m^2, T : Operating temperature (K), I_r : Solar irradiation (W/m^2).

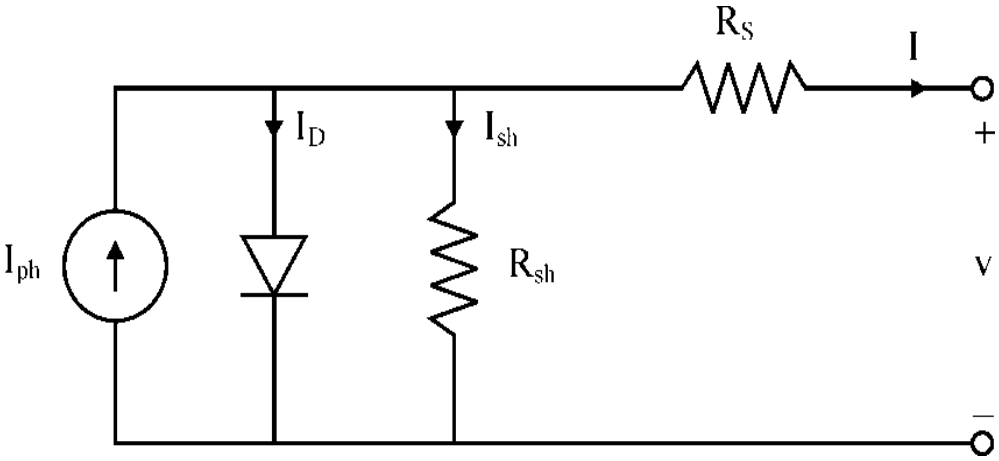

Fig. 2.1 Equivalent Circuit of PV Cell

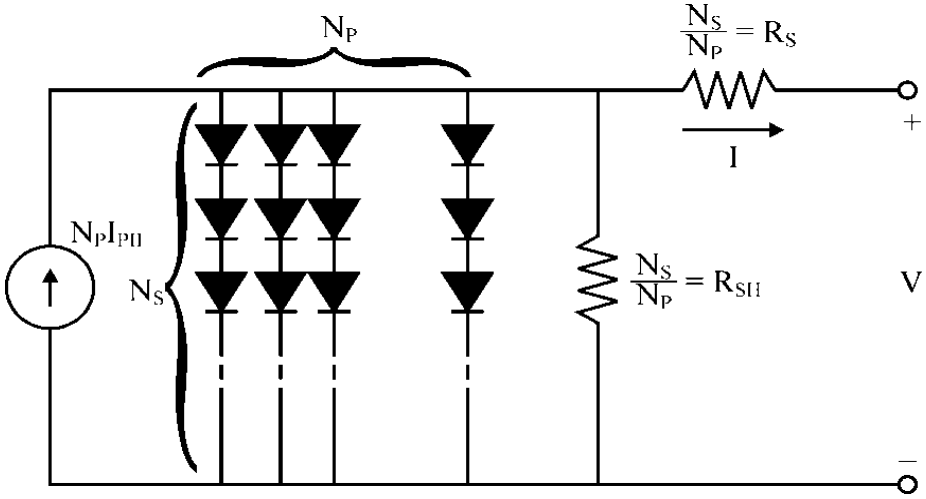

Fig. 2.2 Solar Array Equivalent Circuit

Module reverse saturation current

$$I_{rs} = I_{sc} / \left[\exp\left(qV_{oc} / N_S knT \right) - 1 \right] \quad \ldots.2$$

Here,

q : Electron charge = 1.6 × 10−19C, V_{oc} : Open circuit voltage (V), N_S : Number of cells connected in series, n : Ideality factor of the diode, k : Boltzmann's constant = 1.3805 × 10^{-23} J/K.

The I_0 module saturation current varies with the cell temperature, which is given by:

$$I_0 = I_{rs} \left[\frac{T}{T_r} \right]^3 \exp\left[\frac{q * E_{g0}}{nk} \left(\frac{1}{T} - \frac{1}{T_r} \right) \right] \quad \ldots3$$

Here,

T_r : Nominal temperature = 298.15 K, E_{g0} : Band gap energy of the semiconductor = 1.1 eV

The PV module current output is:

$$I = N_p \times I_{ph} - N_p \times I_0 \times \left[\exp\left(\frac{V / N_s + I \times R_s / N_p}{n \times V_t} \right) - 1 \right] - I_{sh} \quad \ldots4$$

With

$$v_t = \frac{k \times T}{q} \quad \ldots5$$

@2017, IJTRS All Right Reserved

and

$$I_{sh} = \frac{V \times N_p / N_s + I \times R_s}{R_{sh}} \quad \ldots 6$$

N_p : Number of PV modules connected in parallel, R_s : Series resistance (Ω), R_{sh} : Shunt resistance (Ω), v_t : Diode thermal voltage (V).

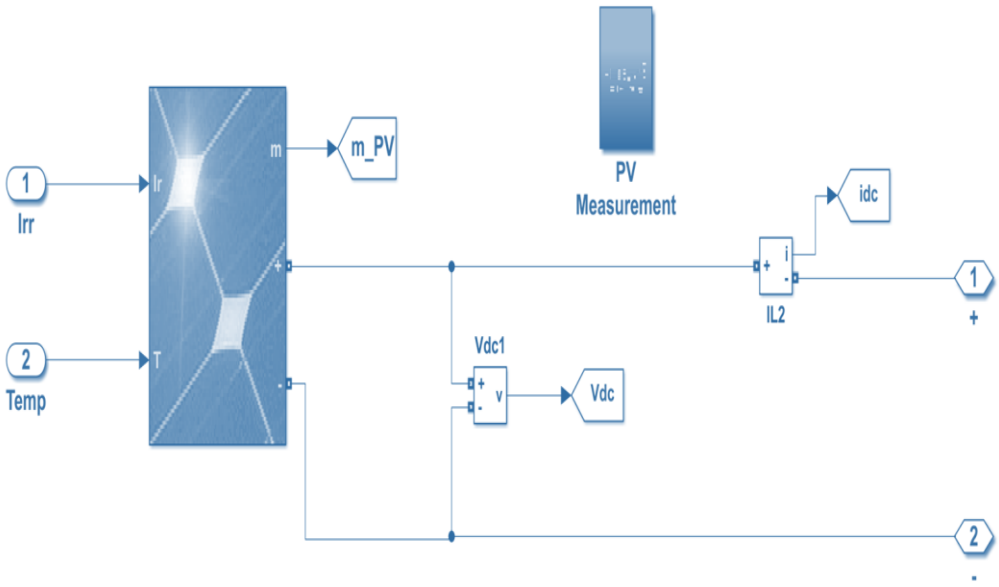

Fig. 2.3 Simulink Model of Solar PV System

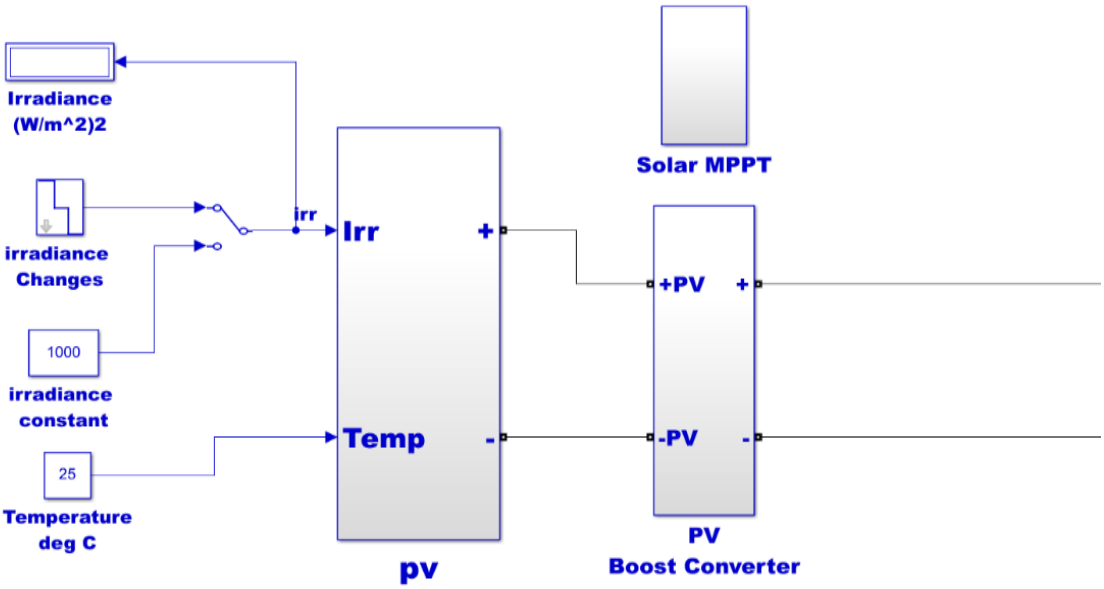

Fig. 2.4 Simulink Model of PV Array with MPPT

3. ARTIFICIAL NEURAL NETWORKS (ANN) METHOD

Artificial Neural Networks (ANNs) are computational models inspired by the human brain, designed to process information through interconnected units called neurons. Organized into layers—input, hidden, and output—they transform data using adjustable weights. ANNs are trained on datasets, enabling them to learn and adapt without explicit programming. The input layer receives data from files or sensors, which is processed through weighted connections to hidden layers, where transformations occur. Finally, the output layer delivers results influenced by these weights. Renowned for their ability to recognize patterns, classify data, and optimize systems, ANNs excel in tasks requiring learning and adaptive problem-solving.

@2017, IJTRS All Right Reserved

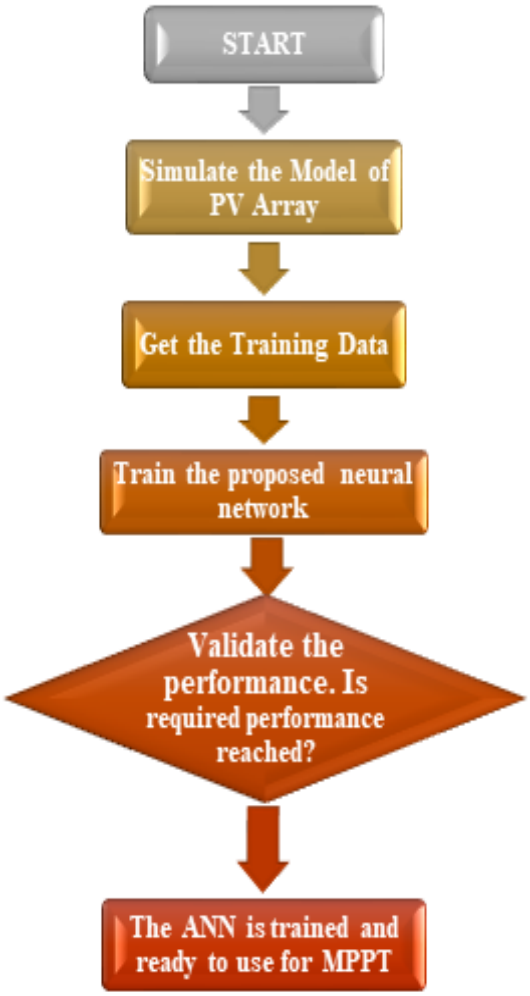

Fig. 3.1 Flow chart for ANN-based MPPT training in SECS

Artificial Neural Networks (ANNs) can be structured as single-layer or multilayer networks, based on the number of hidden layers. They operate using either feedforward or feedback (recurrent) approaches. In feedforward networks, data flows unidirectional from input to output, enabling top-down or bottom-up processing without loops. In contrast, feedback networks allow bidirectional signal flow, forming loops that enhance memory and computational power. ANNs are particularly effective for Maximum Power Point Tracking (MPPT) in solar PV systems, adapting to varying environmental conditions. The Levenberg-Marquardt (LM) algorithm is commonly used to train ANNs using data from PV modules. Figure 5 illustrates the ANN-based MPPT training process.

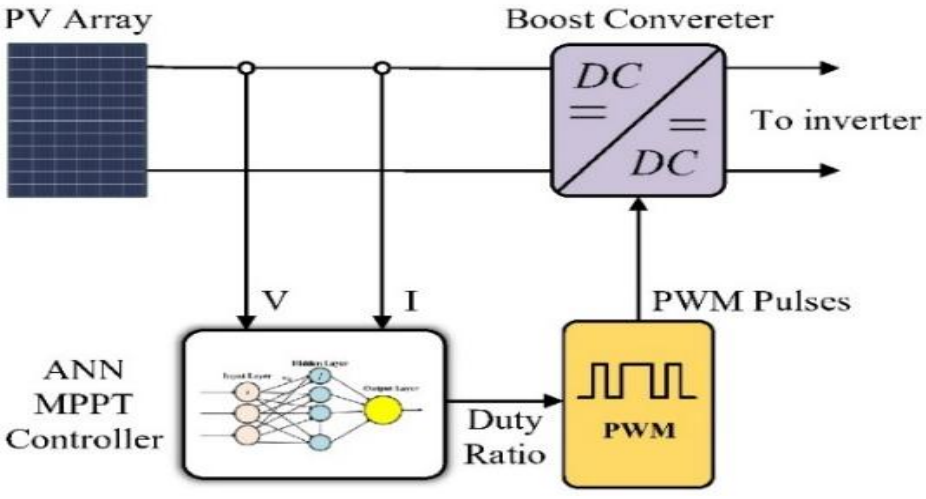

Fig. 3.2 Block Diagram of ANN MPPT Controller

@2017, IJTRS All Right Reserved

An Artificial Neural Network (ANN) comprises interconnected neurons with adjustable weights, organized into input, hidden, and output layers. In PV systems, voltage and current inputs pass through a hidden layer with 15 neurons, where activation functions process data. The output layer optimizes PV performance, aiding MPPT under varying conditions.

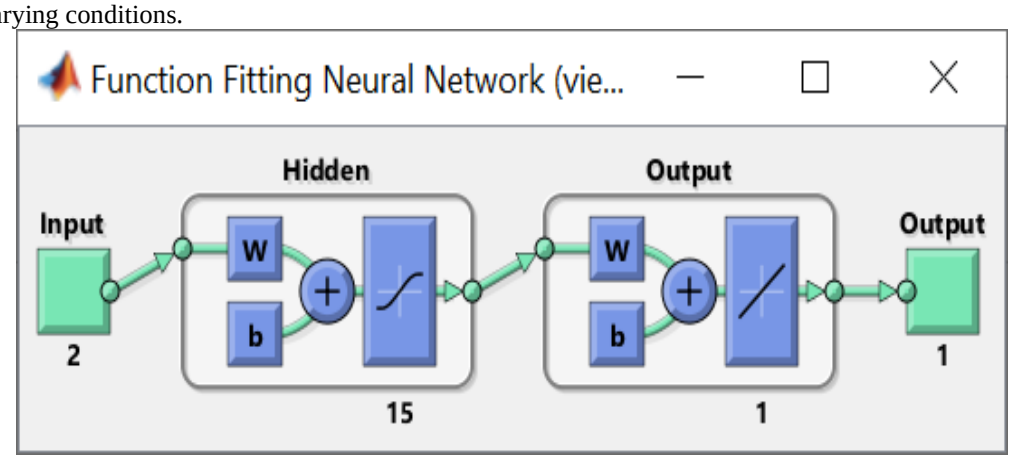

Fig. 3.3 Architecture of LM ANN

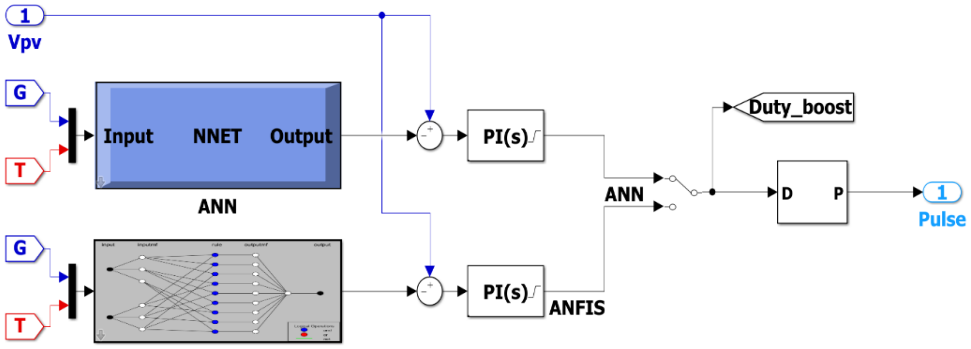

Fig. 3.4 The Developed block of ANN Algorithm

4. ANFIS TRAINING

Figure 8 illustrates the ANFIS model structure, which takes two inputs—PV voltage and PV current—and produces one output, the duty ratio for the boost converter. Fig. 4.1 and 4.2 show the ANFIS testing and training data, generated by comparing the actual voltage of the PV array with the reference voltage from the ANFIS controller. The duty ratio of the DC-DC converter is adjusted to ensure the PV array operates at maximum output. Figures 4.3 and 4.4 display the ANFIS training error and surface viewer. The PI regulator generates the duty cycle based on the voltage error between the reference voltage (Vref) from ANFIS and the measured PV voltage (VPV).

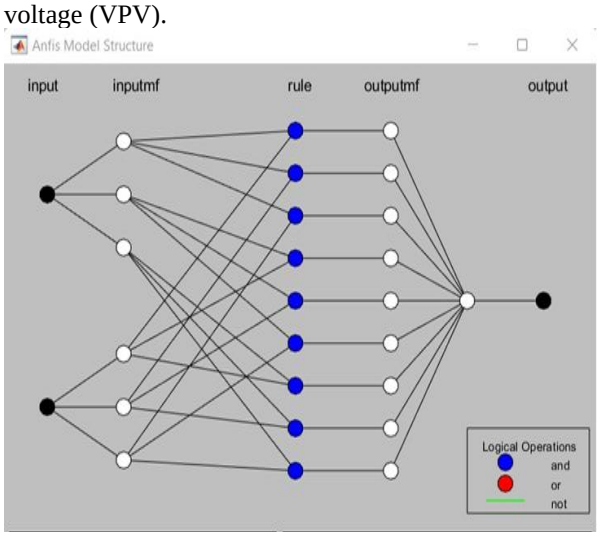

Fig. 4.1 ANFIS Model Structure

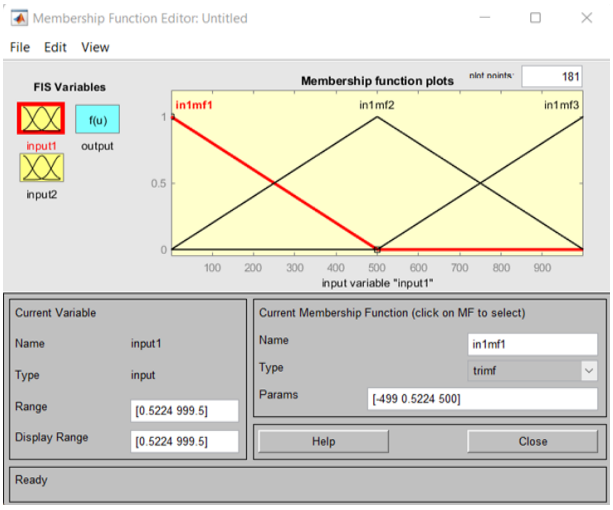

Fig. 4.2 Membership Function for ANFIS based MPPT Controller

@2017, IJTRS All Right Reserved

ISSN Number: 2454-2024(Online)

International Journal of Technical Research & Science

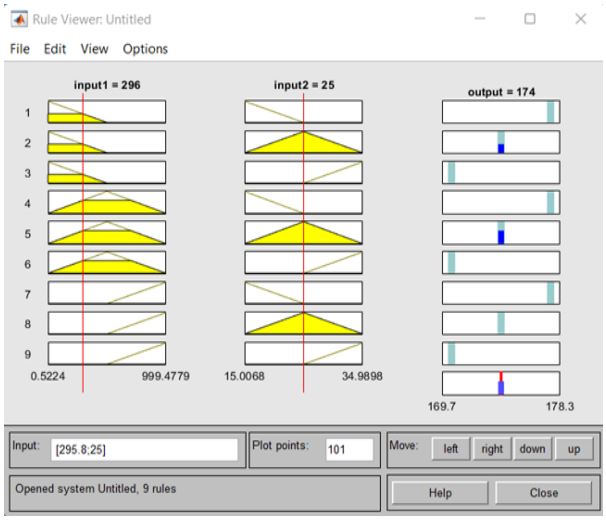

Fig. 4.3 Rules for ANFIS based MPPT Controller

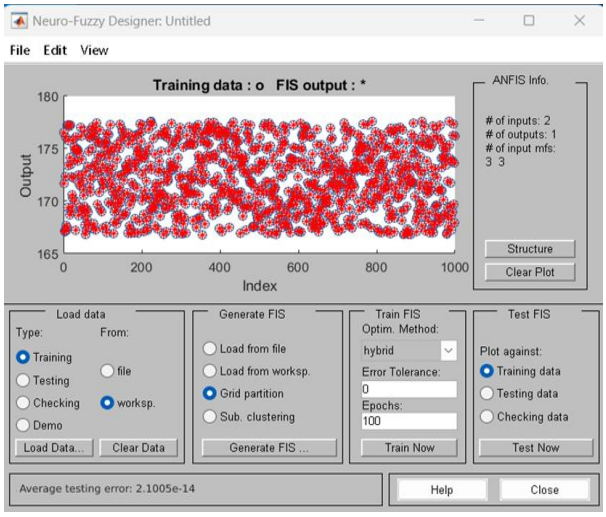

Fig. 4.4 ANFIS Testing Data

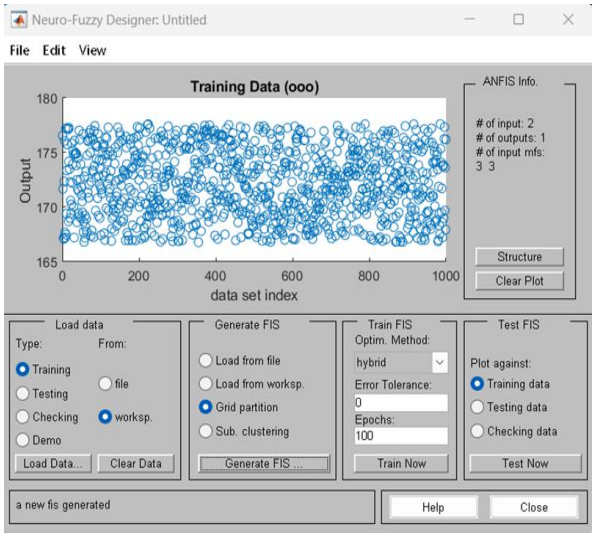

Fig. 4.5 ANFIS Training Data

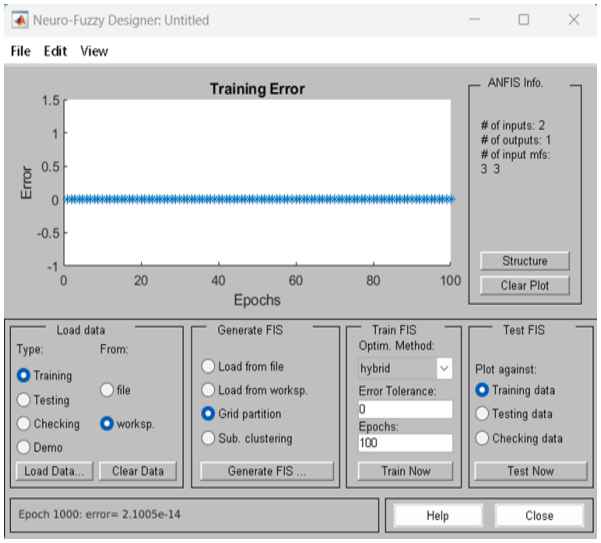

Fig. 4.6 ANFIS Training Error

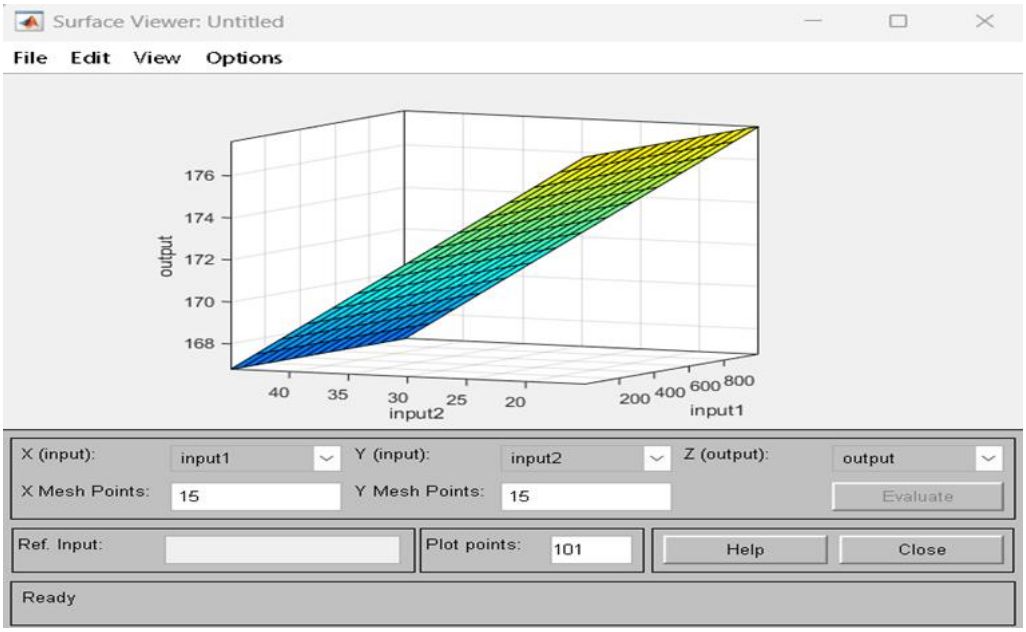

Fig. 4.7 ANFIS Surface Viewer

@2017, IJTRS All Right Reserved

5. SIMULATION RESULT OF AI-BASED MPPT CONTROLLER AT IRRADIANCE STEP CHANGE WITH RESISTIVE LOAD

This simulation study investigates the performance of the proposed system utilizing an ANFIS-based MPPT Controller under step changes in irradiance from 400 to 600 to 800 to 1000 W/m², with a resistive load of 2.5 kW. The simulation covers a duration of 4 seconds, and the results at various stages are presented in the following subsections. These results provide insights into how the system responds to varying solar irradiance levels and assess its efficiency and stability under dynamic environmental conditions. Fig. 4.1 (a) depicts the input irradiance starting at 400 W/m² at t = 0, which steps up to 600 W/m² at t = 1 sec, further up to 800 W/m² at t = 2 sec, and then to 1000 W/m² at t = 3 sec, with the temperature maintained at 25°C, as shown in Fig. 4.1 (b). Throughout the simulation duration, the output voltage of the PV system remains stable at approximately 175 V, with slight variations observed at t = 1 sec, 2 sec, and 3 sec coinciding with the irradiance step changes (400-600-800-1000 W/m²), as illustrated in Fig. 4.1 (c).

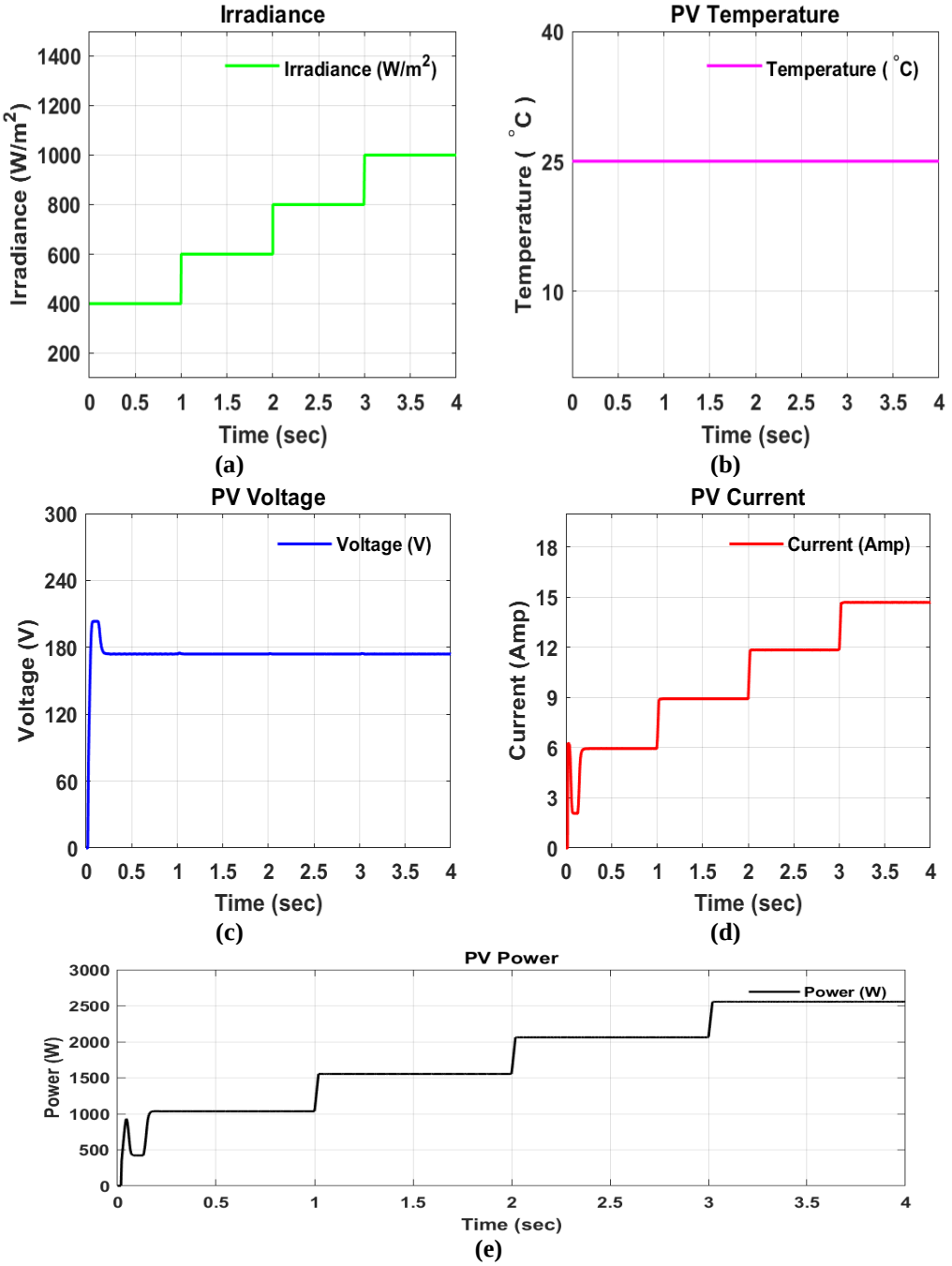

@2017, IJTRS All Right Reserved

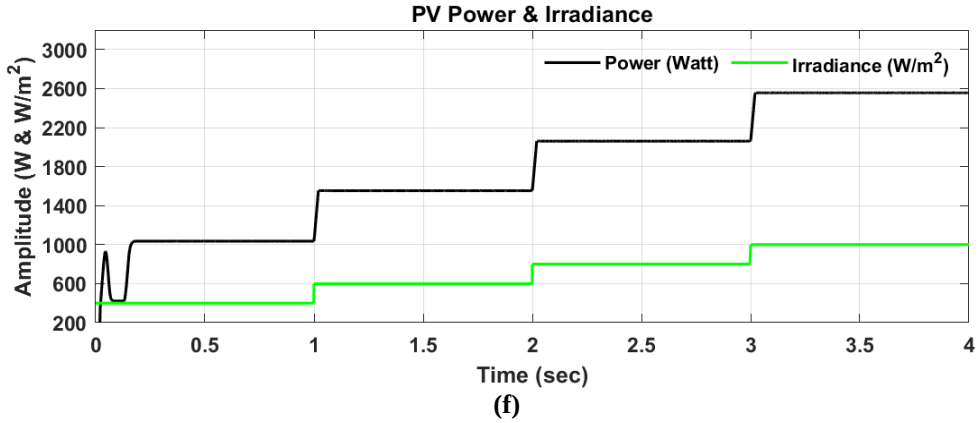

(f)

Fig. 4.1 (a) PV Irradiance (b) PV Temperature (c) PV Voltage, (d) PV Current (e) PV Output Power (f) PV Output Power with Irradiance

Fig. 4.1 (d) displays the PV system's output current, which increases from 6 A at t = 0 to 9 A at t = 1 sec, further increasing to 12 A at t = 2 sec, and then to 14.5 A at t = 3 sec. In Figure 15 (f), the output power of the PV system changes from 1000 W at t = 0 to 1580 W at t = 1 sec, then to 2060 W at t = 2 sec, and finally to 2550 W at t = 3 sec, corresponding to the step changes in irradiance from 400 W/m² to 600 W/m² to 800 W/m² to 1000 W/m².

These figures collectively demonstrate the dynamic response of the PV system to varying irradiance levels, showcasing changes in voltage, current, and power output under different environmental conditions while maintaining stability and efficiency. This section presents the performance of the boost converter under step changes in irradiance (400-600-800-1000 W/m²) with a resistive load. Fig. 4.2 (a) and 4.2 (b) illustrate the constant voltage output of the boost converter, maintained at 500V, alongside the current generated by the ANFIS-based MPPT Controller. These figures depict how the system responds to the stepwise decrease in irradiance levels (400-600-800-1000 W/m²) while supplying a resistive load of 2.5 kW.

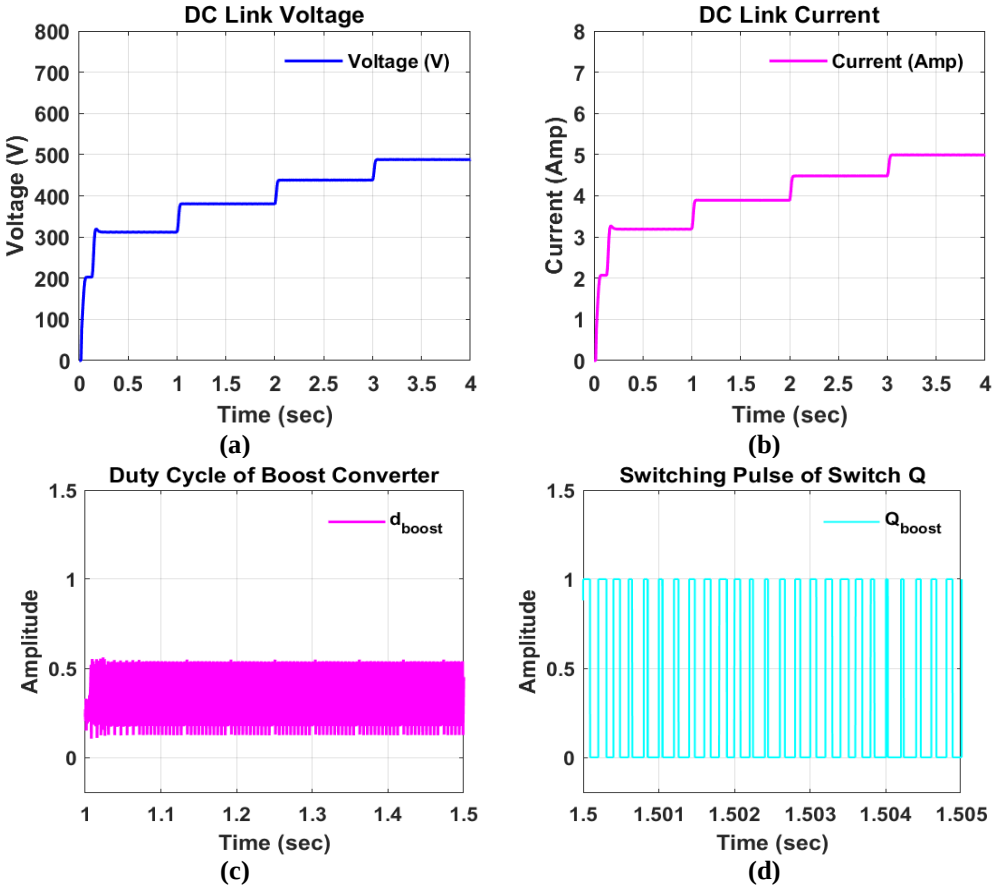

(a) (b) (c) (d)

Fig. 4.2 (a) Boost converter DC link Voltage, (b) Boost converter DC link Current, (c) Duty Cycle of Boost Converter (d) Switching Pulse of Switch Q

@2017, IJTRS All Right Reserved

Fig. 4.2 (c) and 4.2 (d) show the duty cycle of the boost converter's switching pulses. This duty cycle serves as input to the pulse generator, which produces PWM (Pulse Width Modulation) pulses at a switching frequency of 5 kHz. The duty cycle dynamically adjusts in response to changes in irradiance, ensuring efficient modulation of power delivery to the load. These graphical representations collectively demonstrate the operational dynamics of the boost converter and ANFIS-based MPPT Controller system under varying solar irradiance conditions, highlighting their ability to maintain stable output voltage, optimize current delivery, and adjust duty cycles for enhanced energy conversion efficiency.

5. SIMULATION RESULTS UNDER STAIRCASE IRRADIANCE LEVELS AT CONSTANT TEMPERATURE OF 25°C

In this case, stair-case profile of irradiance is used to observe PV output data during varying irradiance condition. The irradiance changes from 1000w/m^2 to 800w/m^2 to 600w/m^2 to 400w/m^2 between time duration of t=0 to t=1.5 sec, t=1.5 to t=3 sec, t=3 to t=4.5 sec & t=4.5 to t=6 sec, respectively. Temperature and load kept constant for whole simulation time. The simulation results are shown in the following figures. Fig. 5.1 shows waveforms of irradiance and temperature applied at the input of PV panel.

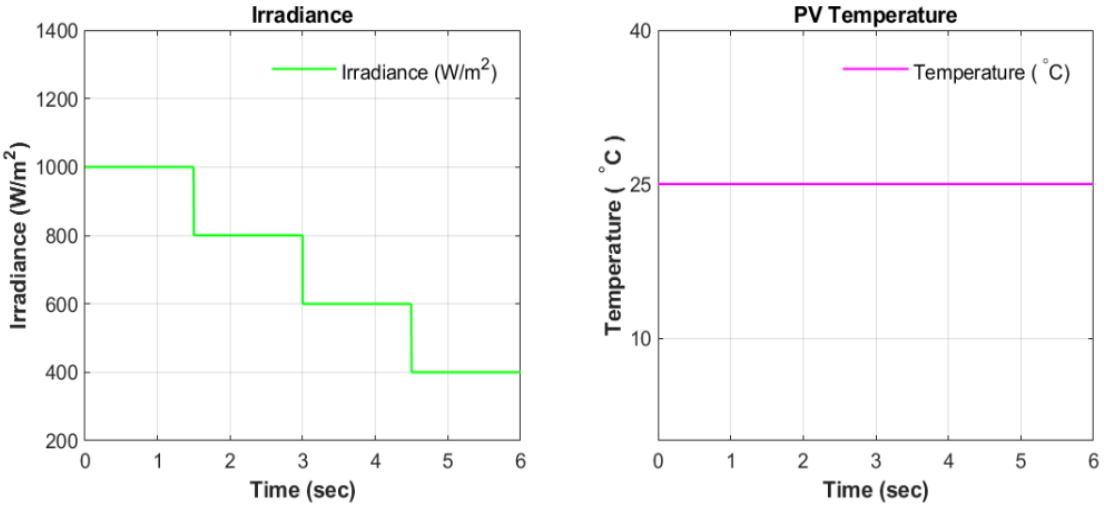

Fig. 5.1 Waveform of Irradiance and Temperature

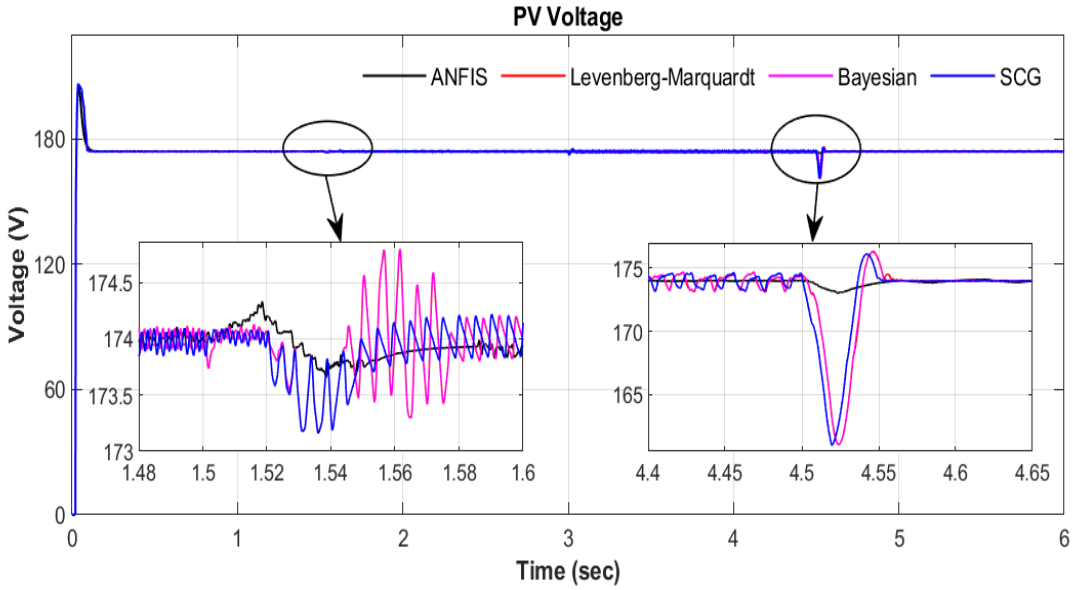

Fig. 5.2 Waveform of PV Voltage

Fig. 5.2 shows, waveform of PV array voltage. As seen by the figure, the PV voltage is maintained at 174V for whole simulation time. First window shows, the response of the algorithms at irradiance changes from 1000W/m^2 to 800w/m^2 between time duration of t=1.48sec to t=1.6 sec. The second window shows, the response at irradiance changes from 600w/m^2 to 400w/m^2 between time duration of t=4.4sec to t=4.65 sec. At this time PV voltage is maintained at its normal value by ANFIS algorithm whereas PV voltage by other algorithms

@2017, IJTRS All Right Reserved

gradually goes down up to 160v for few seconds. Also, a voltage spike can be seen by the other algorithms during irradiance changes from 600w/m^2 to 400w/m^2.

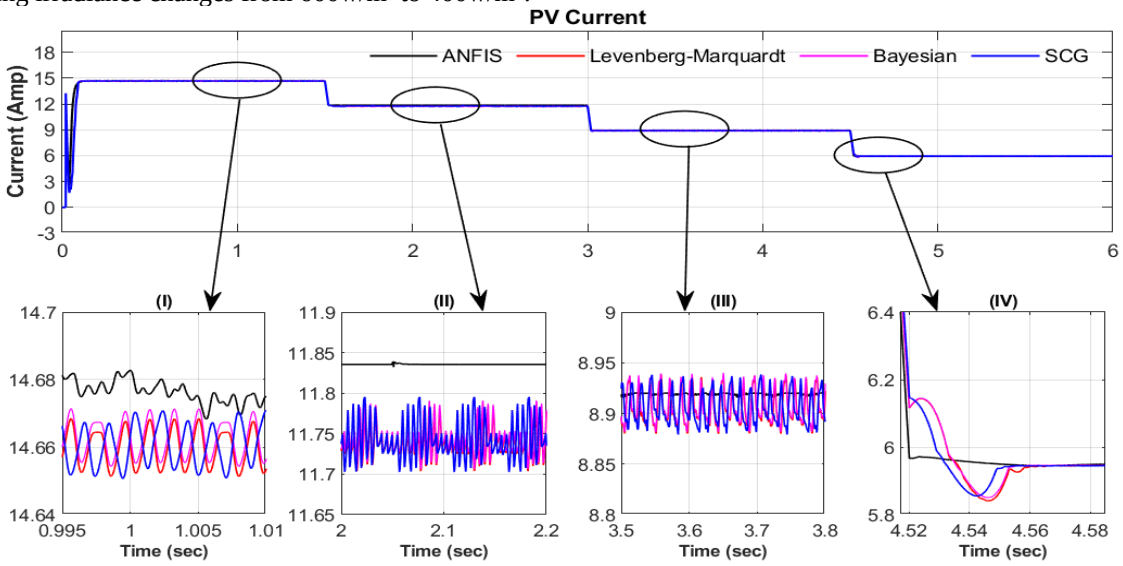

Fig. 5.3 Waveform of PV Current

Fig. 5.3 shows, waveform of PV current generated by PV array. There are four plot windows taken to show the difference among LM neural network, BR network, SCG network and ANFIS network for MPPT algorithms. Window-I is taken between time duration of t=0.995 sec to t=1.01 sec where amplitude of PV current is 14.68amp by ANFIS algorithm and is between 14.65-14.67amp by the remaining algorithms. Window-II is taken between time duration of t=2 sec to t=2.2 sec where amplitude of PV current is 11.84amp by ANFIS algorithm and is between 11.7-11.8amp by the remaining algorithms. Window-III is taken between time duration of t=3.5 sec to t=3.8 sec where amplitude of PV current is 8.925amp by ANFIS algorithm and is between 8.88-8.94amp by the remaining algorithms. Window-IV is taken between time duration of t=4.52 sec to t=4.58 sec where amplitude of PV current is nearly 5.95amp by all the algorithm. The only difference is that when irradiance changes from 600 w/m^2 to 400 w/m^2 the LM, BR and SCG neural network algorithms takes time to maintains its value whereas no time taken by ANFIS algorithm.

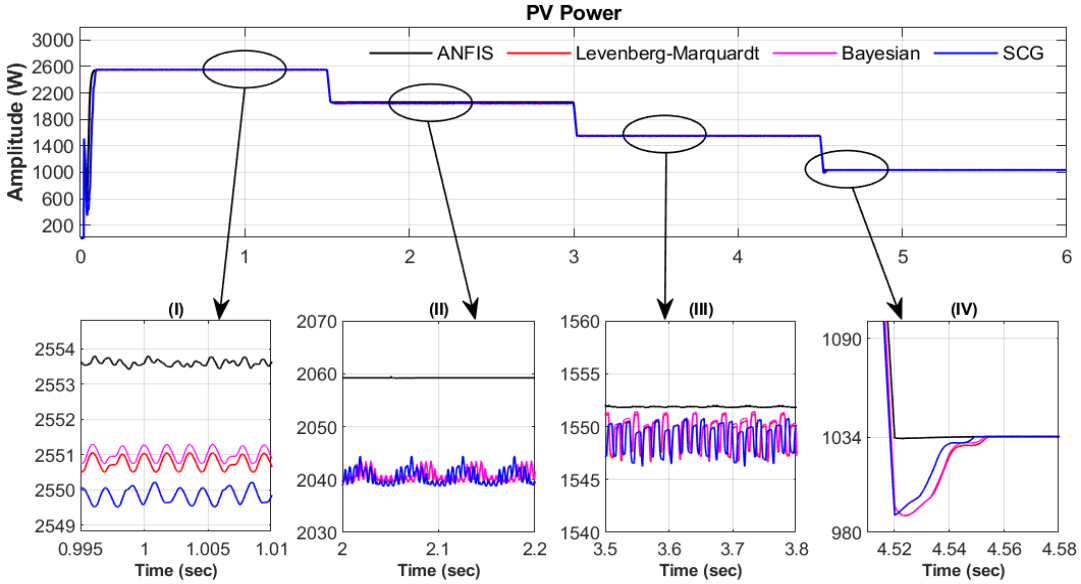

Fig. 5.4 Waveform of PV Output Power

Fig. 5.4 shows the waveform of PV output power at different irradiance conditions. Window-I is taken between time duration of t=0.995 sec to t=1.01 sec where amplitude of PV power is 2554w by ANFIS algorithm, 2551w by LM & BR neural network algorithms and 2550w by SCG network algorithm, as showing in the figure. Window-II is taken between time duration of t=2 sec to t=2.2 sec where amplitude of PV power is 2060w by ANFIS algorithm and 2040W by LM, BR and SCG network algorithms. Window-III is taken between time duration of t=3.5 sec to t=3.8 sec where amplitude of PV power is 1552w by ANFIS algorithm and between 1546-1550W by LM, BR and SCG network algorithms. Window-IV is taken between time duration of t=4.51

@2017, IJTRS All Right Reserved

sec to t=4.58 sec where amplitude of PV power is 1034W by all the algorithms. The only difference is that when irradiance changes from 600 w/m^2 to 400 w/m^2 the LM, BR and SCG neural network algorithms takes time to maintains its value whereas no time taken by ANFIS algorithm.

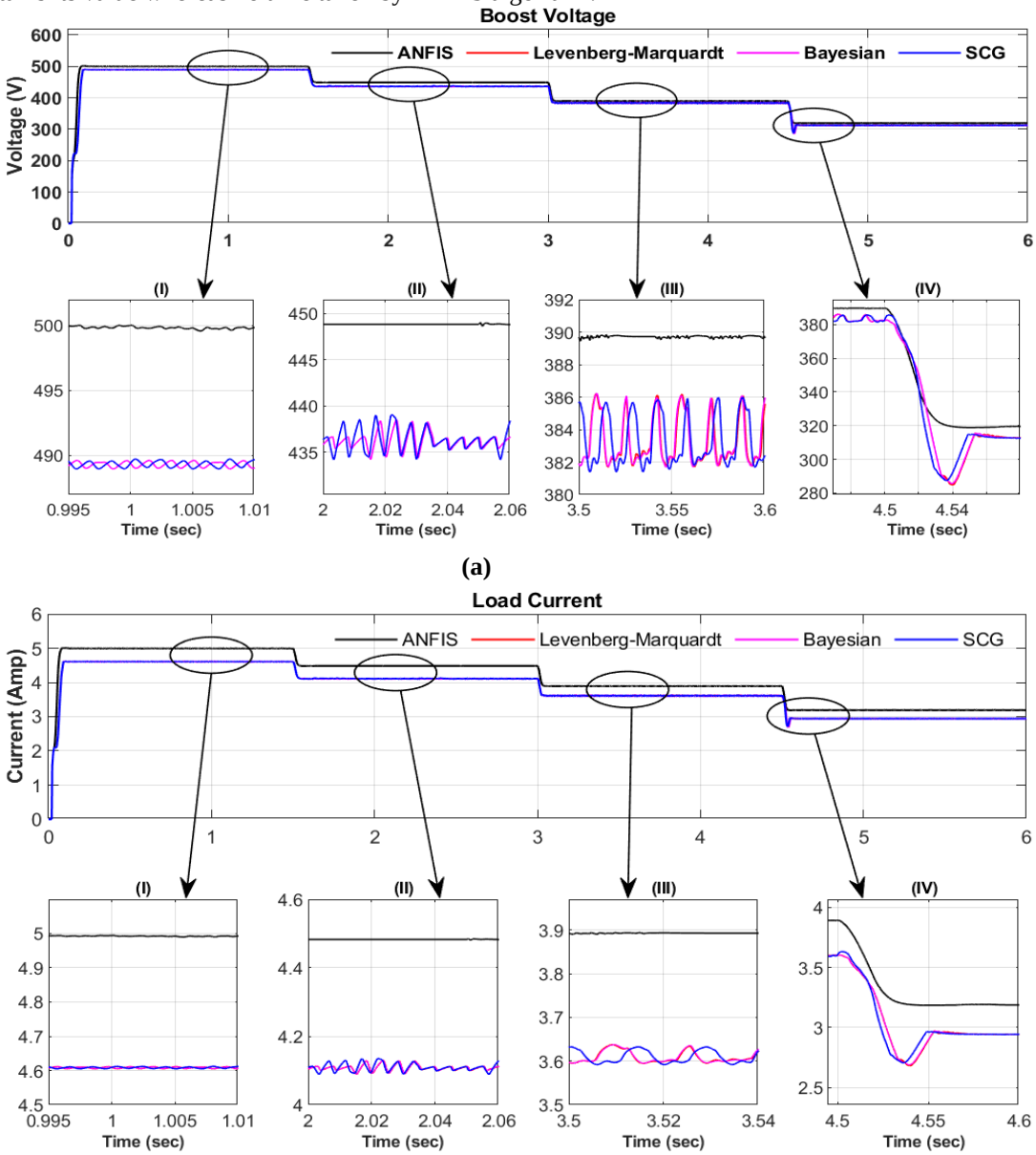

Fig. 5.5 Waveform of (a) Boost Converter Output Voltage and, (b) Load Current

Fig. 5.5 (a) and (b), shows the waveform of boost converter output voltage and load current at different irradiance conditions. In fig. 5.5 (a), Window-I is taken between time duration of t=0.995 sec to t=1.01 sec where amplitude of boost converter output voltage is maintained at 500v by ANFIS algorithm and 490V by LM & BR and SCG network algorithms, as showing in the figure. Window-II is taken between time duration of t=2 sec to t=2.06 sec where amplitude of boost converter output voltage is 449v by ANFIS algorithm and 436V by other neural network algorithms at irradiance of 800w/m^2. Window-III is taken between time duration of t=3.5 sec to t=3.6 sec where amplitude of boost converter output voltage is 390V by ANFIS algorithm and between 381-386V by other neural network algorithms. Window-IV is taken between time duration of t=4.46 sec to t=4.58 sec where amplitude of boost converter output voltage is 320V by all the algorithms.

In fig. 5.5 (b), Window-I is taken between time duration of t=0.995 sec to t=1.01 sec where amplitude of load current is 5amp by ANFIS algorithm and 4.6A by LM & BR and SCG network algorithms, as showing in the figure. Window-II is taken between time duration of t=2 sec to t=2.06 sec where amplitude of load current is 4.5A by ANFIS algorithm and 4.32A by other neural network algorithms at irradiance of 800w/m^2. Window-III is taken between time duration of t=3.5 sec to t=3.54 sec where amplitude of load current is 3.9A by ANFIS algorithm and 3.6A by other neural network algorithms. Window-IV is taken between time duration of t=4.5 sec

@2017, IJTRS All Right Reserved

to t=4.6 sec where amplitude of load current is 3.2A by ANFIS algorithm and 2.98A by other neural network algorithms.

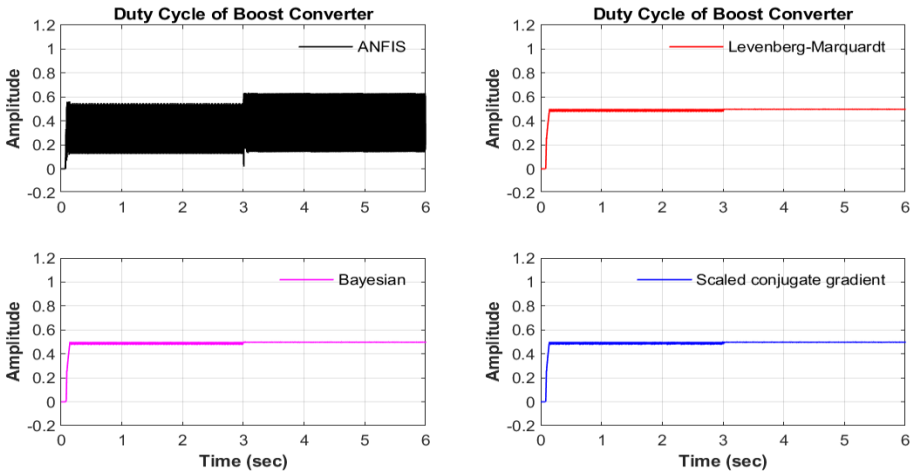

Fig. 5.6 Waveform of Boost Converter Duty Cycle

Fig. 5.6 shows, the waveform of comparison of MPPT algorithms for generating boost converter duty cycle.

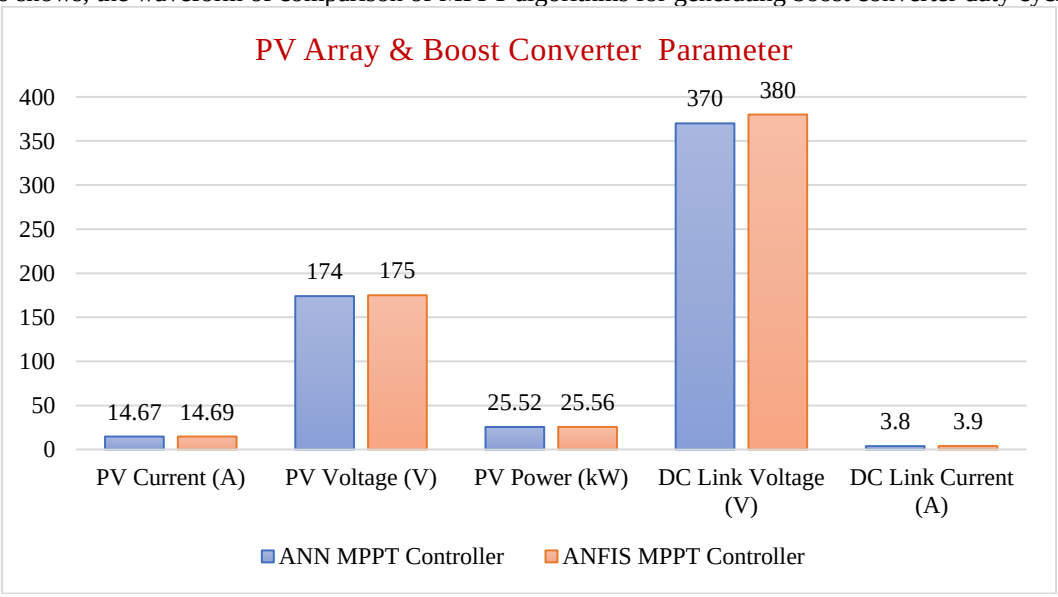

Fig. 5.7 Comparison of ANN and ANFIS based MPPT Controller

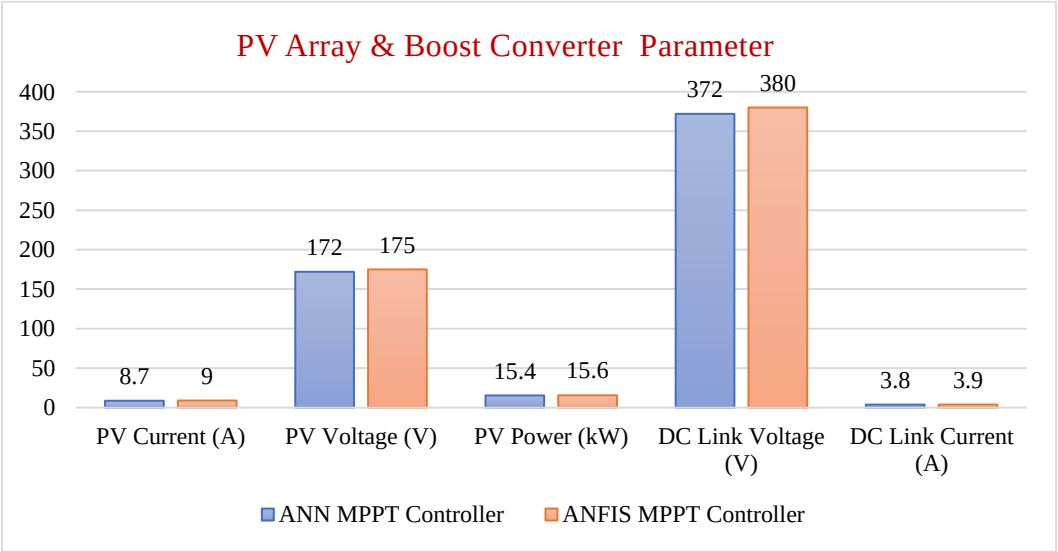

Fig. 5.8 Comparison of ANN and ANFIS based MPPT Controller

@2017, IJTRS All Right Reserved

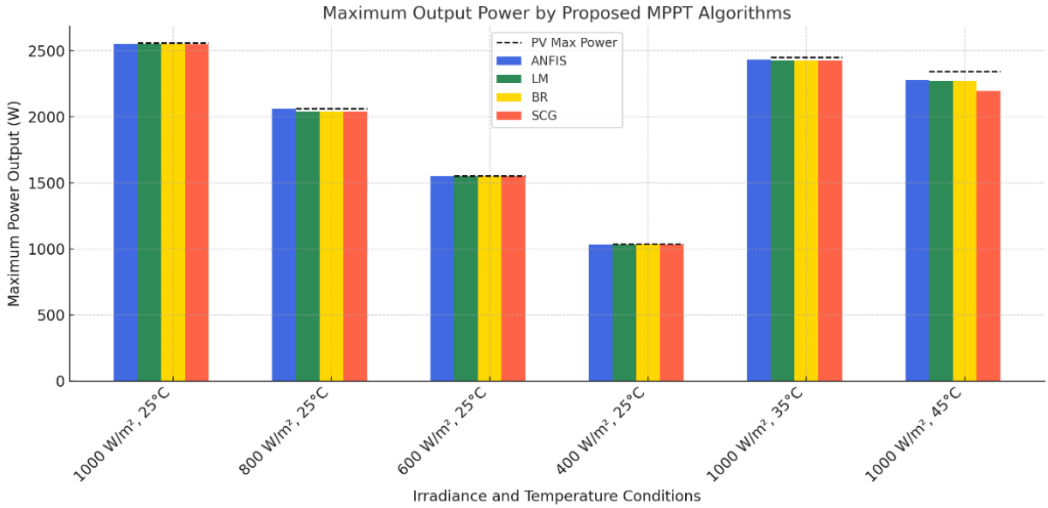

Fig. 5.9 Maximum Output Power by Proposed MPPT Algorithms

The simulated and verified ANFIS-based MPPT Controller for off grid solar PV systems demonstrates superior performance under various input/output conditions. Comparative results indicate that the DC-DC converter for Solar Energy System with the ANFIS-based MPPT Controller outperforms the ANN MPPT Controller.
Table 5.1 and Fig 5.9 present the maximum solar PV power generated by the proposed MPPT algorithms across different irradiation and temperature conditions. Furthermore, Fig. 5.9 depicts the efficiency of these algorithms.

Table-5.1 Maximum Output Power by Proposed MPPT Algorithms

S. No.	Parameters		PV panel maximum output power	Maximum Power by MPPT algorithms (watt)			
	Irr. (w/m^2)	Temp (°C)		ANFIS	LM	BR	SCG
1.	1000	25	2558	2553.9	2550.83	2551.09	2549.81
2.	800	25	2061	2059.14	2040.39	2040.39	2040.39
3.	600	25	1554	1551.97	1548.8	1548.8	1548.8
4.	400	25	1035	1034.37	1034.58	1034.68	1034.17
5.	1000	35	2451	2434	2426.49	2426.49	2426.98
6.	1000	45	2344	2277.66	2272.03	2272.03	2194.21

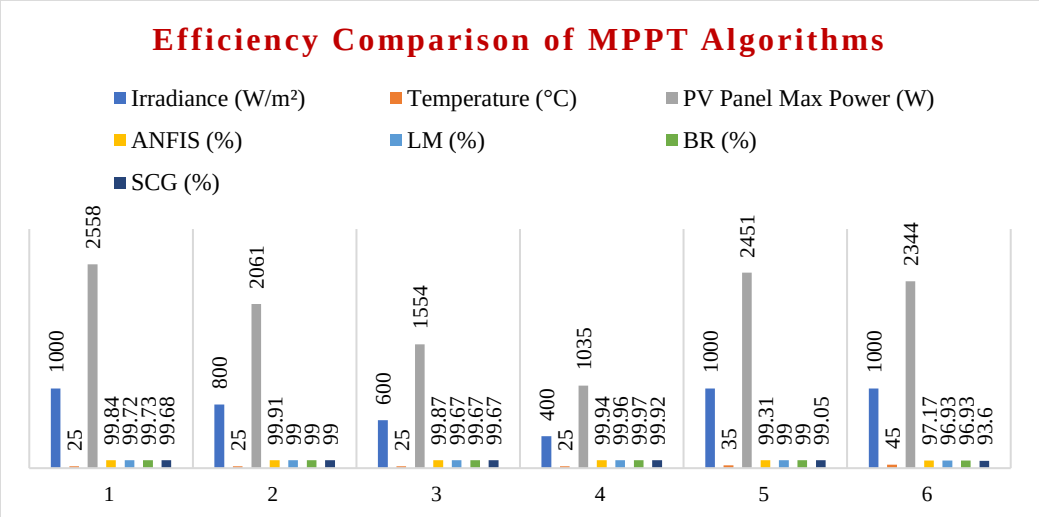

Fig. 5.10 Efficiency of Proposed MPPT Algorithms

@2017, IJTRS All Right Reserved

Table 5.2 clearly shows that the ANFIS algorithm is more effective than other neural network algorithms in extracting maximum power from the solar PV array. Additionally, the LM and BR neural network algorithms exhibit higher efficiency compared to the SCG algorithm. The performance parameters are as follows: 1.0324e-10 for LM, 1.5817e-07 for BR, 5.2169e-04 for SCG, and 2.1005e-14 for ANFIS.

Table-5.2 Comparative Performance Analysis of ANN Algorithms

Parameters	Algorithms			
	ANFIS	**LM**	**BR**	**SCG**
Regression	1	1	1	0.99994
Gradient	….	1.2437e-07	1.0114e-06	0.0089763
Error at middle bin	……	- 1.21e-06	- 1.7e-05	-0.00011
Performance	2.1005e-14	1.0324e-10	1.5817e-07	5.2169e-04
Momentum Parameter	…….	1e-07	50000	-
Epochs	1000	1000	1000	342

The ANFIS algorithm demonstrates superior performance with a zero-mean squared error compared to the LM, BR, and SCG algorithms. When considering dataset training, the correlation between input and output, and the zero-mean squared error, the ANFIS algorithm outperforms the others.

CONCLUSION

This study evaluates the performance of ANFIS-based MPPT controllers compared to various AI techniques for photovoltaic (PV) systems under diverse operational conditions. Both simulations and real-time applications highlight the consistent superiority of the ANFIS controller, especially in scenarios with fluctuating input irradiance. The results demonstrate that the ANFIS-based MPPT controller achieves better optimization of solar energy systems, surpassing traditional ANN-based controllers in output voltage, current, and power. Additionally, it provides smoother duty ratios and enhanced overall efficiency. Regression analysis shows coefficients of 1, 1, 0.99994, and 1 for the LM, BR, SCG, and ANFIS algorithms, with respective performance values of 1.0324e-10, 1.5817e-07, 5.2169e-04, and 2.1005e-14.

REFERENCES

[1] Hu J, Lim B-H, Tian X, et al. “A Comprehensive Review of Artificial Intelligence Applications in the Photovoltaic Systems”. CAAI Artificial Intelligence Research, Vol. 3, 2024, https://doi.org/10.26599/AIR.2024.9150031

[2] Alias S. S, et al. “Maximizing solar power generation through conventional and digital MPPT techniques: a comparative analysis”. Scientific Reports, Vol. 14, 2024.

[3] Mazumdar D, et al. “Optimizing MPPT Control for Enhanced Efficiency in Sustainable Photovoltaic Microgrids: A DSO-Based Approach”. International Transactions on Electrical Energy Systems, Vol. 12, pp. 1-19, 2024.

[4] Md Tahmid Hussain., et. al., “An Evaluation of ANN Algorithm Performance for MPPT Energy Harvesting in Solar PV Systems,” Sustainability 2023, 15(14), 11144; https://doi.org/10.3390/su151411144, 2023.

[5] Roy. R. B., et. al., “A Comparative Performance Analysis of ANN Algorithms for MPPT Energy Harvesting in Solar PV System,” IEEE Access, vol. 9, no. 2, pp. 102137–102152, 2022.

[6] M. Rokonuzzaman, M. K. Mishu, N. Amin, M. Nadarajah, R. B. Roy, K. S. Rahman, A. M. Buhari, S. Binzaid, M. Shakeri, and J. Pasupuleti, ‘‘Self-sustained autonomous wireless sensor network with integrated solar photovoltaic system for internet of smart home-building (IoSHB) applications,’’ Micromachines, vol. 12, no. 6, p. 653, Jun. 2021, doi: 10.3390/mi12060653.

[7] N. Karami, N. Moubayed, and R. Outbib, ‘‘General review and classification of different MPPT techniques,’’ Renew. Sustain. Energy Rev., vol. 68, pp. 1–18, Feb. 2017, doi: 10.1016/j.rser.2016.09.132.

[8] M. Rokonuzzaman, M. Shakeri, F. A. Hamid, M. K. Mishu, J. Pasupuleti, K. S. Rahman, S. K. Tiong, and N. Amin, ‘‘IoT-enabled high efficiency smart solar charge controller with maximum power point tracking— Design, hardware implementation and performance testing,’’ Electronics, vol. 9, no. 8, p.

@2017, IJTRS All Right Reserved

1267, Aug. 2020, doi: 10.3390/electronics9081267.
[9] M. K. Mishu, M. Rokonuzzaman, J. Pasupuleti, M. Shakeri, K. S. Rahman, S. Binzaid, S. K. Tiong, and N. Amin, ‘‘An adaptive TE-PV hybrid energy harvesting system for self-powered IoT sensor applications,’’ Sensors, vol. 21, no. 8, p. 2604, Apr. 2021, doi: 10.3390/s21082604
[10] C. H. Basha and C. Rani, ‘‘Different conventional and soft computing MPPT techniques for solar PV systems with high step-up boost converters: A comprehensive analysis,’’ Energies, vol. 13, no. 2, p. 371, Jan. 2020.
[11] L. Chen and X. Wang, ‘‘Enhanced MPPT method based on ANN-assisted sequential Monte–Carlo and quickest change detection,’’ IET Smart Grid, vol. 2, no. 4, pp. 635–644, Dec. 2019.
[12] J. A. Gow and C. D. Manning, “Development of a photovoltaic array model for use in power-electronics simulation studies,” IEE Proceedings: Electric Power Applications, vol. 146, no. 2, pp. 193–200, 2020.
[13] Roy. R. B., et. al., “A Comparative Performance Analysis of ANN Algorithms for MPPT Energy Harvesting in Solar PV System,” IEEE Access, vol. 9, no. 2, pp. 102137–102152, 2021.
[14] S. Sharma; R. Jangid and K. Parikh “Development of Intelligent Control Strategy for Power Quality Improvement of Hybrid RES Using AI Technique” International Journal of Technical Research and Science, vol. VIII, Issue II, Feb. 2023.
[15] M. Rokonuzzaman, M. K. Mishu, N. Amin, M. Nadarajah, R. B. Roy, K. S. Rahman, A. M. Buhari, S. Binzaid, M. Shakeri, and J. Pasupuleti, ‘‘Self-sustained autonomous wireless sensor network with integrated solar photovoltaic system for internet of smart home-building (IoSHB) applications,’’ Micromachines, vol. 12, no. 6, p. 653, Jun. 2021, doi: 10.3390/mi12060653.
[16] L. Jhala et al., “Development of Control Strategy for Power Management in Hybrid Renewable Energy System” International Journal of Technical Research and Science, vol. VI, Issue XII, Dec. 2021.
[17] N. Karami, N. Moubayed, and R. Outbib, ‘‘General review and classification of different MPPT techniques,’’ Renew. Sustain. Energy Rev., vol. 68, pp. 1–18, Feb. 2017, doi: 10.1016/j.rser.2016.09.132.
[18] S. Kumar: R. Jangid and K. Parikh “Comparative Performance Analysis of Adaptive Neuro-Fuzzy Inference System (ANFIS) & ANN Algorithms Based MPPT Energy Harvesting in Solar PV System.” International Journal of Technical Research and Science, vol. 8, Issue 3, March 2023.
[19] M. Rokonuzzaman, M. Shakeri, F. A. Hamid, M. K. Mishu, J. Pasupuleti, K. S. Rahman, S. K. Tiong, and N. Amin, ‘‘IoT-enabled high efficiency smart solar charge controller with maximum power point tracking— Design, hardware implementation and performance testing,’’ Electronics, vol. 9, no. 8, p. 1267, Aug. 2020, doi: 10.3390/electronics9081267.
[20] M. K. Mishu, M. Rokonuzzaman, J. Pasupuleti, M. Shakeri, K. S. Rahman, S. Binzaid, S. K. Tiong, and N. Amin, ‘‘An adaptive TE-PV hybrid energy harvesting system for self-powered IoT sensor applications,’’ Sensors, vol. 21, no. 8, p. 2604, Apr. 2021, doi: 10.3390/s21082604.
[21] R. Jangid; J.k Maherchandani; V.K Yadav and R.K Swami, “Energy Management of Standalone Hybrid Wind-PV System”, Journal of Intelligent Renewable Energy Systems (John Wiley & Sons, Inc.) Pages 179- 198, 2022
[22] R. Jangid; J.k Maherchandani; R.R. Joshi and B.D Vairagi, “Development of Advance Energy Management Strategy for Standalone Hybrid Wind & PV System Considering Rural Application”, IEEE 2nd International Conference on Smart Systems and Inventive Technology, Organized by Francis Xavier Engineering College during November 27-29, 2019 at Tirunelveli, India.
[23] C. H. Basha and C. Rani, ‘‘Different conventional and soft computing MPPT techniques for solar PV systems with high step-up boost converters: A comprehensive analysis,’’ Energies, vol. 13, no. 2, p. 371, Jan. 2020.
[24] Y. Joshi; J.k Maherchandani; V.K Yadav; R. Jangid; S. Vyas and S.S Sharma, “Performance Improvement of Standalone Battery Integrated Hybrid System” IEEE 7th International Conference on Electrical Energy Systems (ICEES), Organized by Sri Sivasubramaniya Nadar College of Engineering during 11-13 Feb. 2021at Chennai, India
[25] L. Chen and X. Wang, ‘‘Enhanced MPPT method based on ANN-assisted sequential Monte–Carlo and quickest change detection,’’ IET Smart Grid, vol. 2, no. 4, pp. 635–644, Dec. 2019.

@2017, IJTRS All Right Reserved

@2017, IJTRS All Right Reserved